Turkish Journal of Electrical Engineering & Computer Sciences

http://journals.tubitak.gov.tr/elektrik/

Research Article

Turk J Elec Eng & Comp Sci
(2020) 28: 2288 – 2302

doi:10.3906/elk-2001-141

Simplified model predictive current control of non-sinusoidal low power brushless DC machines

Alireza LAHOOTI ESHKEVARI, Hossein TORKAMAN*
Faculty of Electrical Engineering, Shahid Beheshti University, Tehran, Iran

Received: 30.01.2020 • **Accepted/Published Online:** 27.04.2020 • **Final Version:** 29.07.2020

Abstract: Several strategies have been proposed to control nonsinusoidal brushless DC machines (BLDCMs). However, high electromagnetic torque ripple and current overshoots occur in commutation times, which are significant problems of those strategies such as for hysteresis current controllers. This paper proposes a model predictive strategy to solve the above issues. It is simple and straightforward. Moreover, it reduces the motor torque ripple significantly and improves the response rate of the control system to the load torque variation in comparison with the conventional technique. The torque varies smoothly, and the performance of the system at commutation time is improved by eliminating the adverse effects of commutation times on the machine's current and torque. This method also operates better than the conventional controller in medium switching frequencies. The novelty of this strategy is that it employs a model predictive strategy to realize the above claims. The real implementation possibility and performance of the controller are investigated by simulations for a 60-V/180-W/300-RPM BLDCM. This paper also compares the proposed current controller with the conventional controller. The results show that the torque ripple reduces 50%, and the brake and response times are improved.

Key words: BLDC motor drive, predictive control, current control, synchronous motor, nonsinusoidal back-emf, speed control

1. Introduction

Brushless DC motors (BLDCMs) are a type of synchronous AC machines (SMs) with nonsinusoidal or trapezoidal back-emf waveform. BLDCMs usually includes 3 Hall sensors, suitable for rotor position detecting, reproducing signals of each phase current and back-emf voltage, and even determining the status of the inverter switches. This machine has concentrated stator windings with a 120° coil span. The BLDC rotor consists of permanent magnet (PM) material, which covers a 180° pole arc. Therefore, the induced back-emf is trapezoidal with 120° flat top regions. As discussed previously [1], the BLDCM provides 15% more power and torque capability than PMSMs. This feature is convenient in many applications, such as electric vehicle (EV) propulsion systems.

Control methods of BLDCMs are classified into 2 groups: 2-phase conduction mode and 3-phase conduction mode strategies [1]. In the first group, the machine works with 3-phase rectangular currents and 120° conduction zones; however, in the second group, it operates with rectangular currents and 180° conduction zones. Studies show that 3-phase conduction mode has a better torque-speed capability than the first method in the constant power region [1]. Various advance speed controllers and advance converters [2–5], either with a

*Correspondence: h_torkaman@sbu.ac.ir

sensor or sensorless [6–9], have been introduced by researchers to date. The first strategy is called the hysteresis method and works based on the relationship between machine torque and current. This control loop requires 3 sensors to measure each phase current [10, 11]. Thus, the number of necessary sensors may be a challenge in an actual system. Some studies have covered this problem by proposing different solutions. The number of sensors can be reduced only by measuring the DC link current [11] or using the wavelet theory [7]. Current control strategies also employ hysteresis modulation. Therefore, their control quality depends on the bandwidth of hysteresis controllers. High-resolution bandwidth requires higher switching frequencies, which may exceed the practical constraints. Of course, the torque ripple is increased by reducing the switching frequency.

All presented solutions can be developed for 4-switch 3-phase inverters [12, 13]. A 4-switch inverter has fewer semiconductors than the traditional six-switch inverters, which reduces the overall cost of a BLDCM driver significantly [12]. In 4-switch inverters, 1 phase of the motor is connected to the midpoint of DC-link capacitors, and this phase current never becomes zero due to its back-emf voltage. Xia et al. [12] worked on the commutation times problem in these inverters and appended 2 regulating vectors in each sampling interval. As a result, the corresponding phase current was controlled by controlling the operation time of regulating vectors in each sampling period.

A conventional direct torque control strategy has been developed for BLDCMs [14, 15]. It focused on torque ripple minimization. The aim is to use a suitable switching state to reach the desired torque value [16–18]. Similar to induction and synchronous machines, direct torque control (DTC) has been implemented for BLDC machines [19–29]. DTC dominates the torque and flux directly by using 2 hysteresis controllers. These controllers pick the best switching state based on a predefined look-up table. It is notable that the switching events in sinusoidal machines differ from those in nonsinusoidal machines. Accordingly, the development of classical DTC for a BLDC machine is slightly complex if compared with other AC machines. The switching frequency is not constant in traditional DTC. Ozturk et al. [24] explained the disadvantages of conventional DTC for BLDCMs, and they suggested a modified direct torque controller that controls just the torque value. It does not affect the motor flux.

In recent years, predictive strategies have been promoted for electrical machines and power electronic converters rapidly [27–38]. Predictive controllers improve control performance compared to traditional methods. The model predictive control is based on the prediction of the system output and the minimization of a cost function to discover an optimal control input. The predictive controller requires estimating the future value of controlled parameters and a cost function for determining the best switching event. The need for solving the cost function has been resolved using the deadbeat approach. The predictive approach has been proposed earlier for BLDCMs [31]. However, Valle et al. [31] employed predictive theory for adding a new modulation method to the traditional current control strategy. Applying vector control strategies to BLDCMs is slightly complex due to the lack of sinusoidal back-emf voltage and accessing the neutral point of the stator windings. Furthermore, the modulation method is different for BLDCMs.

Predictive control of BLDC machines has been discussed less than that of other AC machines. Therefore, the present paper aims to investigate a different and straightforward predictive current controller for BLDCMs. This theory is developed for six-switch inverters. Although this controller incorporates hysteresis modulation, it shows better performance at medium switching frequencies. Additionally, the proposed controller provides lower torque ripple in comparison with the conventional current controller, since it does not affect the torque directly. The proposed controller first predicts the future value of the motor currents. Then it compares the result with references that are generated by the speed controller. The contribution of this strategy is to use

model predictive theory to improve the performance of the conventional current controller, was not presented before. In comparison with the conventional model predictive control, which requires solving a minimization problem of the cost function, our strategy does not need this, and it is straightforward. Using the hysteresis modulation makes this strategy easier to implement. Numerical simulations in MATLAB/Simulink evaluate the possibility and performance of the proposed approach for a typical low-power 60-V/180-W/300-RPM BLDCM.

2. The principle of predictive control for the BLDCM drive

2.1. Model of the BLDCM

Figure 1 shows a BLDCM connected to a six-switch inverter. Figure 1 also depicts the BLDCM equivalent circuit. It includes 3 phases, where each phase comprises a resistor (R_s), an inductor (L_s), and an independent voltage source, indicating the stator winding resistance, the stator winding inductance, and the back-emf voltage, respectively. This model also represents the mutual inductance between each phase (M). It is assumed that the machine never becomes saturate, and the components of 1 phase are identical to those of another phase. Iron losses are also assumed to be negligible. According to these assumptions, (1) can be obtained, which corresponds to the machine model [11].

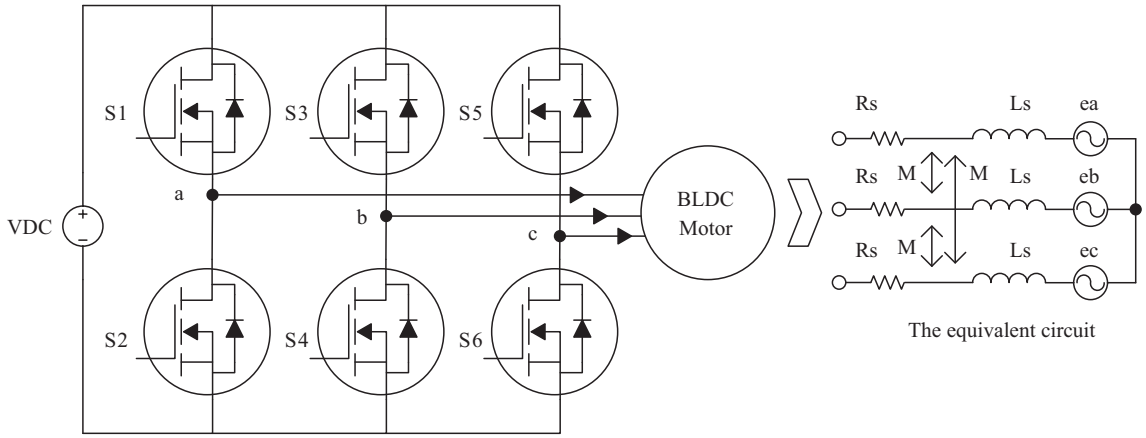

Figure 1. The equivalent circuit of the BLDC machine and the 3-phase inverter.

$$\begin{bmatrix} u_{sa} \\ u_{sb} \\ u_{sc} \end{bmatrix} = \begin{bmatrix} R_s & 0 & 0 \\ 0 & R_s & 0 \\ 0 & 0 & R_s \end{bmatrix} \begin{bmatrix} i_a \\ i_b \\ i_c \end{bmatrix} + \begin{bmatrix} L_s - M & 0 & 0 \\ 0 & L_s - M & 0 \\ 0 & 0 & L_s - M \end{bmatrix} \frac{d}{dt} \begin{bmatrix} i_a \\ i_b \\ i_c \end{bmatrix} + \begin{bmatrix} e_a \\ e_b \\ e_c \end{bmatrix} \tag{1}$$

In (1), the $\begin{bmatrix} u_{sa} & u_{sb} & u_{sc} \end{bmatrix}^T$ indicates the inverter output voltages and $\begin{bmatrix} i_a & i_b & i_c \end{bmatrix}^T$ denotes stator currents. Equation (2) is a classical equation relating the rotor speed to the motor electromagnetic torque. ω_r, T_e, T_L, J, and B indicate the rotor mechanical speed, the electromagnetic torque, the load torque, the inertia, and the friction coefficient, respectively. If the friction coefficient is assumed to be zero, equation (2) can be represented by (3).

$$T_e = T_L + J\frac{d}{dt}\omega_r + B\omega_r \tag{2}$$

$$\omega_r = \frac{1}{J}\int (T_e - T_L)\, dt = \frac{1}{J}\int \left(\sum_{x=a,b,c} T_x - T_L \right) dt \tag{3}$$

In this machine, the electromagnetic torque depends on each phase current. In 2-phase conduction mode, the current is passed through 2 phases at each switching interval, and so the total generating torque can be determined by (4), where K_t is the BLDCM torque constant [11]. Due to the above assumptions, the current of active phases is identical and it is assumed to be I.

$$T_e = \sum_{x=a,b,c} T_x = K_t \left(\sum_{x=a,b,c} I_x \right) = 2K_t I \tag{4}$$

The back-emf amplitude depends on the rotor electrical speed according to (5), where K_e and ω_e indicate the back-emf constant and the rotor electrical speed, respectively.

$$e_{abc} = K_e \omega_e \tag{5}$$

The BLDCM also includes Hall sensors. It is conceivable to use its logic output signals for obtaining torque and back-emf. Table 1 shows different states of these Hall sensors and their relation to the torque and back-emf values. Due to this feature, the proposed model predictive approach determines the values of electromagnetic torque and back-emf voltage. As mentioned above, the electromagnetic torque relates to the phase currents and based on Table 1 it is possible to determine which phase produces this torque value. Consequently, it is possible to identify in which phase current passes.

Table 1. The relationships between Hall sensors and back-emf voltage and torque values.

(Ha,Hb,Hc)	(ea, eb, ec)	(Ta,Tb,Tc)	Rotor position (Deg.)	Sector
(0,0,1)	(0,-1,1)	(0,1,1)	-30 - 30	1
(1,0,1)	(1,-1,0)	(1,1,0)	30 - 90	2
(1,0,0)	(1,0,-1)	(1,0,1)	90 - 150	3
(1,1,0)	(0,1,-1)	(0,1,1)	150 - 210	4
(0,1,0)	(-1,1,0)	(1,1,0)	210 - 270	5
(0,1,1)	(-1,0,1)	(1,0,1)	270 - 330	6

2.2. Principle of the proposed strategy

Figures 2a and 2b show the block diagram of a conventional hysteresis current controller and the proposed model predictive strategy, respectively. The traditional current controller tries to equalize the rotor speed with the reference speed by forcing each phase current to follow their reference values, as depicted in Figure 2a. Figure 2b illustrates the block diagram of the proposed model predictive current controller. At first, the control unit measures the instantaneous phase current, the state of the Hall sensors, the rotor mechanical speed, and the DC-link voltage value (V_{dc}). Calculations are done in the $\alpha\,\beta$ stationary reference frame. Hence, the reference frame of measured currents is converted to the $\alpha\,\beta$ frame by using Clark transformation. Equation (6) shows

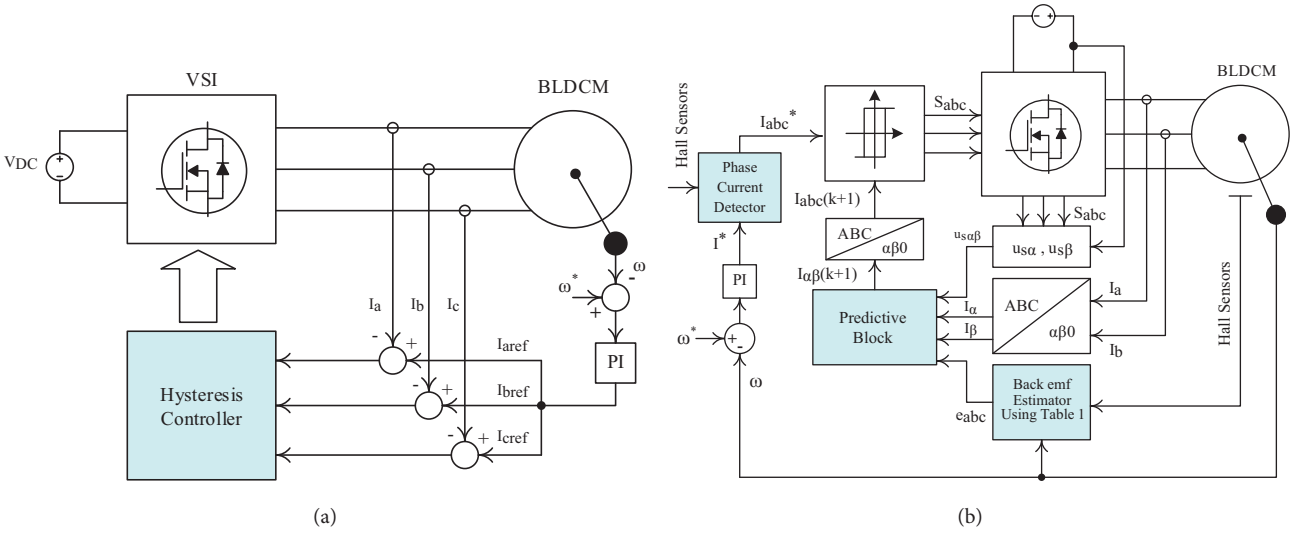

Figure 2. The block diagram of the (a) conventional current controller, (b) model predictive current controller.

the Clark transformation. Under balance condition where $g_a + g_b + g_c = 0$, equation (6) can be simplified as represented by (7).

$$\begin{bmatrix} g_\alpha \\ g_\beta \end{bmatrix} = \frac{2}{3} \begin{bmatrix} 1 & -\frac{1}{2} & -\frac{1}{2} \\ 0 & \frac{\sqrt{3}}{2} & -\frac{\sqrt{3}}{2} \end{bmatrix} \begin{bmatrix} g_a \\ g_b \\ g_c \end{bmatrix} \tag{6}$$

$$\begin{bmatrix} g_\alpha \\ g_\beta \end{bmatrix} = \begin{bmatrix} 1 & 0 \\ \frac{1}{\sqrt{3}} & \frac{2}{\sqrt{3}} \end{bmatrix} \begin{bmatrix} g_a \\ g_b \end{bmatrix} \tag{7}$$

The predictive control unit also requires the values of the back-emf waveforms. The motor back-emf voltages are obtained using the status of Hall sensors and Table 1, as shown in Figures 3a and 3b. This solution solves the neutral-point accessing problem. Estimated back-emf voltages must convert to the $\alpha\,\beta$ reference frame.

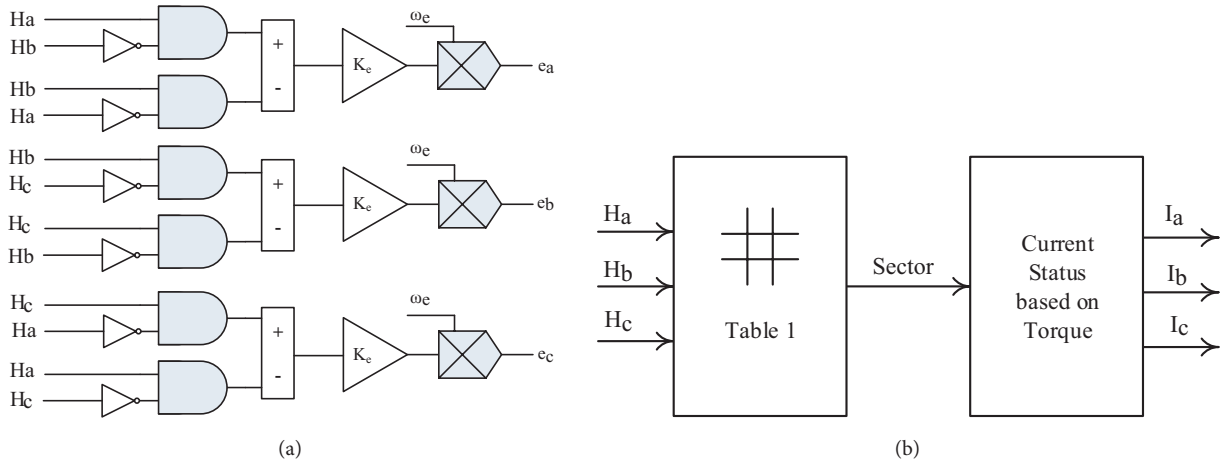

Figure 3. The block diagram of (a) the back-emf estimator block, (b) the phase current detector block.

Additionally, based on (1), the inverter output voltage must be measured or calculated. The inverter output voltage value is deduced by using the DC link voltage value and the inverter switching state. Because the proposed algorithm is placed in the 2-phase conduction mode category, the valid and possible switching events differ from those in the 3-phase conduction mode, as illustrated in Figures 4a and 4b. By performing some algebraic manipulations (8) and (9) can be deduced, where $S_1 - S_6$ shows the switching state of power switches [11]. Their values can be 1 or 0.

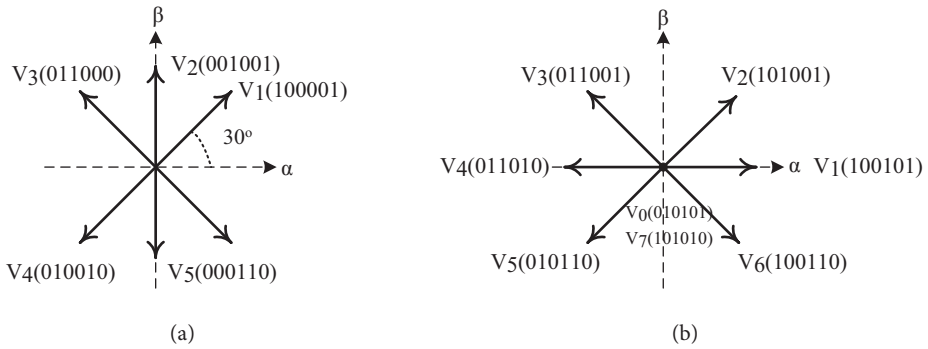

Figure 4. The possible switching states in (a) the 2-phase conduction mode, (b) the 3-phase conduction mode.

$$u_{s\alpha} = \frac{\sqrt{3}}{2} V_{dc} \left(S_1 \left(S_6 + S_4 \right) - S_2 \left(S_3 + S_5 \right) \right) \tag{8}$$

$$u_{s\beta} = \frac{1}{2} V_{dc} \left(S_6 \left(S_1 + S_3 \right) + S_2 \left(S_3 - S_5 \right) - S_4 (S_5 + S_1) \right) \tag{9}$$

Equation (1) can be rewritten in $\alpha\beta$ form, as represented in (10), where $L = L_s - M$. The forward Euler approach is used to convert the continuous form of (10) to the discrete form of (12), where (i_α, i_β), $(u_{s\alpha}, u_{s\beta})$, (e_α, e_β), and T_s denote the stator current, the inverter output voltage, the back-emf voltages, and the sampling period, respectively.

$$\begin{bmatrix} u_{s\alpha} \\ u_{s\beta} \end{bmatrix} = \begin{bmatrix} R_s & 0 \\ 0 & R_s \end{bmatrix} \begin{bmatrix} i_\alpha \\ i_\beta \end{bmatrix} + \begin{bmatrix} L & 0 \\ 0 & L \end{bmatrix} \frac{d}{dt} \begin{bmatrix} i_\alpha \\ i_\beta \end{bmatrix} + \begin{bmatrix} e_\alpha \\ e_\beta \end{bmatrix} \tag{10}$$

$$\frac{dX}{dt} = \frac{X\left(k+1\right) - X\left(k\right)}{T_s} \tag{11}$$

$$\frac{L_s}{T_s} \begin{bmatrix} i_\alpha \left(k+1\right) - i_\alpha \left(k\right) \\ i_\beta \left(k+1\right) - i_\beta \left(k\right) \end{bmatrix} = \begin{bmatrix} u_{s\alpha}(k) \\ u_{s\beta}(k) \end{bmatrix} - R_s \begin{bmatrix} i_\alpha \left(k\right) \\ i_\beta \left(k\right) \end{bmatrix} - \begin{bmatrix} e_\alpha \left(k\right) \\ e_\beta \left(k\right) \end{bmatrix} \tag{12}$$

By simplifying (12), (13) can be determined, which demonstrates the instantaneous current value in the $(k+1)^{th}$ sampling interval. The predictive block in Figure 2b employs (13) in order to estimate the instantaneous current value in the $(k+1)^{th}$ sampling instant.

$$\begin{bmatrix} i_\alpha \left(k+1\right) \\ i_\beta \left(k+1\right) \end{bmatrix} = \frac{T_s}{L_s} \left(\begin{bmatrix} u_{s\alpha} \left(k\right) \\ u_{s\beta} \left(k\right) \end{bmatrix} - \begin{bmatrix} e_\alpha \left(k\right) \\ e_\beta \left(k\right) \end{bmatrix} \right) + \left(1 - \frac{R_s T_s}{L_s} \right) \begin{bmatrix} i_\alpha \left(k\right) \\ i_\beta \left(k\right) \end{bmatrix} \tag{13}$$

The purpose of the predictive strategy is to equalize the value of $i_{\alpha\beta}(k+1)$ with the reference value. To generate the reference value of the above current components, the rotor speed is measured and compared with the speed reference value and the resulting error passes through a PI controller, as shown in Figure 2a. The reference current limit is set to be 1.5 times the rated current due to governing restrictions on motor windings. I^* indicates the amplitude of the reference current; however, the reference current waveforms must be reproduced based on the rotor location. This can be realized by using the state of the Hall sensors and Table 1. The phase current detector block generates the reference currents by using the state of the Hall sensors, as demonstrated in Figure 3b. Therefore, 3 reference values relevant to the current of each phase (A, B, and C) are produced. The reference and the predicted currents are fed to the modulation block, which incorporates 3 hysteresis controllers. These modulators determine the suitable switching state of each phase separately, and they obey (14) as their rule, where $i = a, b, c$. The bandwidth of hysteresis controllers is obtained by the sampling/switching frequency. For this analysis 2% bandwidth is selected.

$$\begin{cases} I_i^* - I_i(k+1) > Upper\ Band \rightarrow & S_i = 1 \\ I_i^* - I_i(k+1) < Lower\ Band \rightarrow & S_i = 0 \end{cases} \tag{14}$$

Proper commands, which originate from the output of hysteresis controllers, are applied to a six-switch inverter. To summarize the process of this suggested strategy, Figure 5 illustrates the flowchart of this proposed algorithm. In section 3, simulations and comparative evaluations are presented for a typical BLDC machine.

3. Results and analysis

3.1. The speed-time characteristic

Table 2 shows the system specifications and Figures 6a and 6b display the speed waveform of the simulated conventional and proposed strategy under constant torque. As can be seen, the rotor speed follows its reference value precisely in both current controllers. In this case, the speed command is changed from 150 rpm to 300 rpm at 0.05 s. The speed controller error is 2% in the conventional current controller. However, this error is decreased to below 1% in the predictive controller. The proposed controller improves the speed accuracy up to 50%. Figures 6c and 6d show the zoomed version of the figures.

3.2. The torque characteristic

Figures 7a and 7b show the effect of torque variation in both strategies. In this case, the torque command is varied from 5 N.m to 2.5 N.m at 0.1 s. Although the electromagnetic torque follows the reference value in both plans, the amount of electromagnetic torque ripple in the predictive algorithm is smaller than that in the conventional current controller. Although the peak to peak value of the electromagnetic torque ripple in the traditional current controller is about 1 N.m, it is reduced to approximately 0.5 N.m using the introduced strategy. Thus, the predictive controller reduces the amount of torque ripple 50%. The other parameter that is improved by using the proposed approach is the torque response time. The predictive controller decreases this value from 80 μs to 72 μs, as shown in Figure 8a. This torque characteristic makes the BLDCM operation smoother. Although the difference between the time waveforms is 8 μs, as can be seen from Figure 8a, the change in electromagnetic torque in the predictive strategy is smoother than that in the hysteresis method. The difference between the response time and the settling time of the torque curve is about 320 μs for the predictive control, while it is about 440 μs for the conventional method. When the torque value is decreased from full

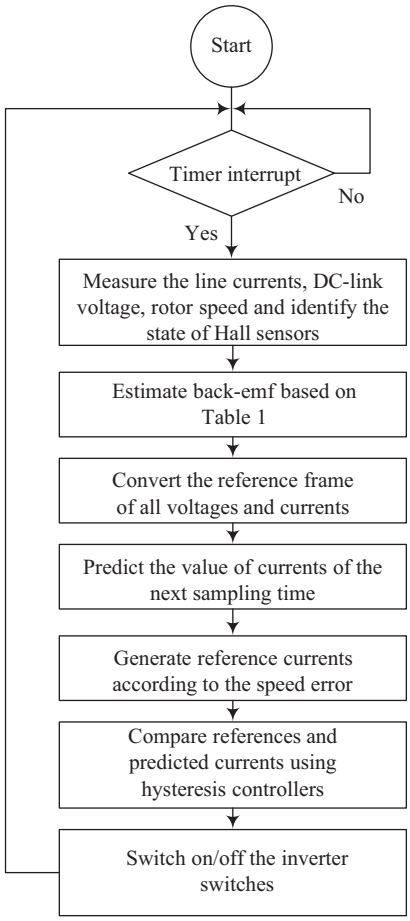

Figure 5. The flowchart of the proposed model predictive current controller for the BLDCM drive.

load (5 N.m) to half load (2.5N.m), the developed torque is reduced rapidly with the smooth slope, as shown in Figure 8a. It is different for the conventional controller, as shown in Figure 8b.

3.3. The effect of switching frequency and commutation time

The performance of the traditional current controller heavily relies on the switching frequency and the narrower hysteresis band. Therefore, the presented strategy improves the quality of the control loop at medium sampling frequencies. As an example, if the conventional current controller operates with the 80-kHz sampling frequency, it reveals much better performance than with the 40-kHz sampling frequency. However, in this case, the proposed predictive algorithm works with 40-kHz switching frequency well. Therefore, the driver equipped with this predictive controller has less switching losses than the conventional current controller because of the switching frequency reduction. It can be inferred from the above discussion that the proposed controller improves efficiency. Other parameters such as the phase current waveforms and the back-emf voltages are depicted in Figures 9a and 9b. As expected, the back-emf voltage has a trapezoidal waveform. Speed increasing or speed decreasing affects the magnitude and frequency of this waveform. The fluctuation elimination from the commutation time is 1 of the most critical items for the current waveforms.

1. Settling time minus the action time.

Table 2. The system specifications.

System parameter	Value
DC link voltage (V)	60
Stator resistance (Ω)	0.64
Stator inductance (mH)	1
Stator mutual inductance (mH)	0.25
Rated voltage (V)	60
Rated current (A)	4.5
Rated torque (N.m)	5
Rated speed (rpm)	300
Rated power (W)	180
Sampling interval (μs)	25
Torque constant (N.m/A)	1.25
Back-emf constant (V/rpm)	0.0667
Pole pairs	8
J (Kg.m^2)	0.0008

Table 3. A comparative study between the conventional and predictive current controllers.

	Methods	
Parameters	Conventionalhysteresis	Predictive control
Speed controller accuracy	Low	High
Speed error	2%	$< 1\%$
$\Delta T_{e_{max}} / T_{e_{rated}}$	20%	10%
$\Delta T_{e_{Peak\ to\ Peak}}$ @ rated torque	1 N.m	2 N.m
Commutation fluctuation	High	Negligible
Torque smoothness	Poor	High
Torque response time (response to reference changing)	80μs	72μs
$(t_s - t_a)$ for torque step change[1]	440μs	320μs
Braking time	1.67ms	1.57ms
Dependency on the sampling frequency	High	Medium
Converter switching loss	Higher	Lower
Efficiency	Lower	Higher

3.4. The brake mode and bidirectional operation

The braking time is another test case. Figures 10a and 10b show the performance of each strategy for decreasing the speed from 250 rpm to zero at constant load torque (5 N.m). According to Figures 10a and 10b, it takes 1.57 ms for the proposed strategy and 1.67 ms for the conventional controller to change the speed from 250 rpm to zero. As a result, the response speed is 5% increased. To summarize the above discussion, Table 3 is organized to compare both the predictive and the conventional current controller.

Another test case is relevant to the reverse speed effect. In this case, the BLDCM operates at full load and the rated speed. The rotor direction is changed using the speed command. Both methods work accurately,

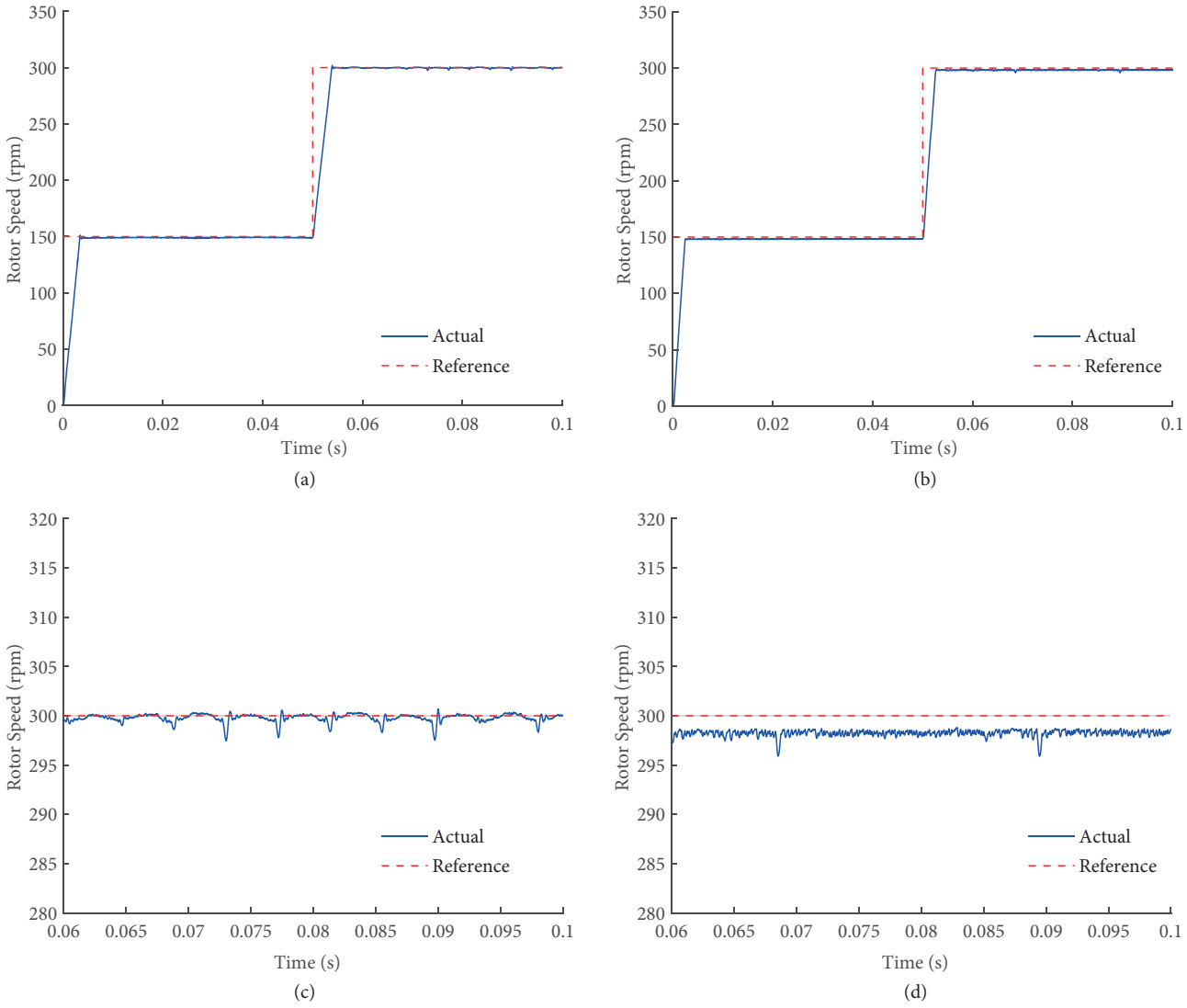

Figure 6. The motor speed waveform with the constant torque of 2.5 N.m: (a) proposed strategy, (b) conventional, (c) item (a) with zoom, (d) item (b) with zoom.

but the predictive current controller provides lower electromagnetic torque ripple. Figures 11a and 11b show the results of this case.

3.5. Stability analysis

The motor parameters might be changed during operation. Basic predictive controllers are sensitive to system parameter changes when their stability is placed at risk. This problem originates from the operating principle of the predictive controllers, where the model of the system is required. Constant values for all system parameters are chosen. If the system parameter changes, the controller error can be increased. This section identifies the stability range of the proposed predictive current controller subject to the stator winding resistance and the stator winding inductance. The variations in speed error and torque ripple are illustrated in Figures 12a and 12b in terms of the stator winding resistance variation and stator inductance variation. The stator winding

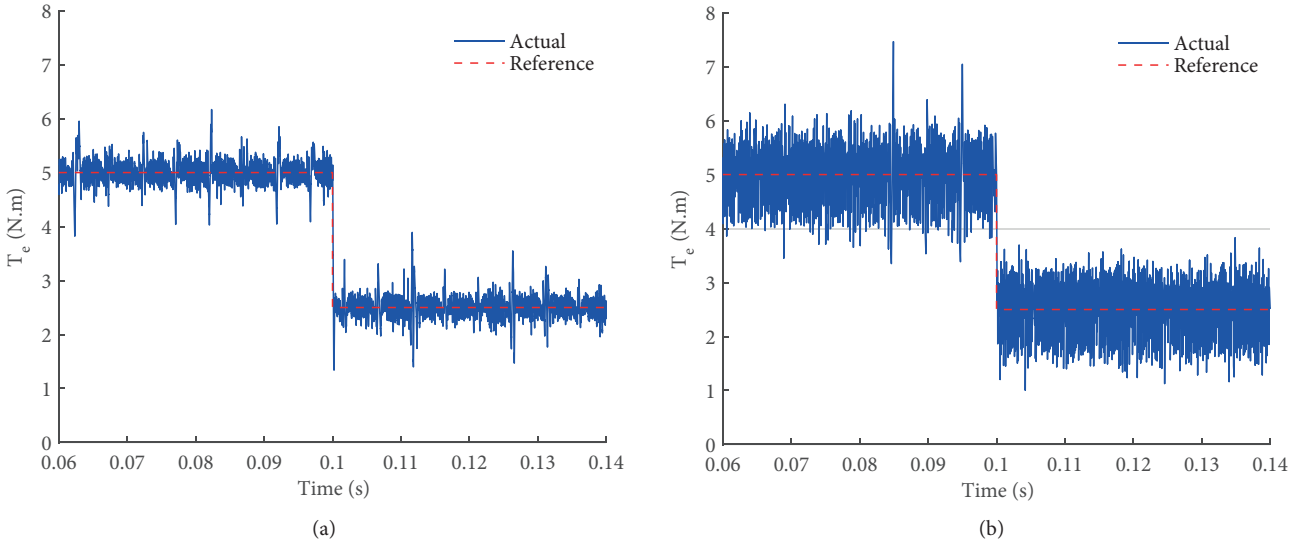

Figure 7. The electromagnetic torque waveform with the constant speed of 250 rpm: (a) the proposed approach, (b) conventional.

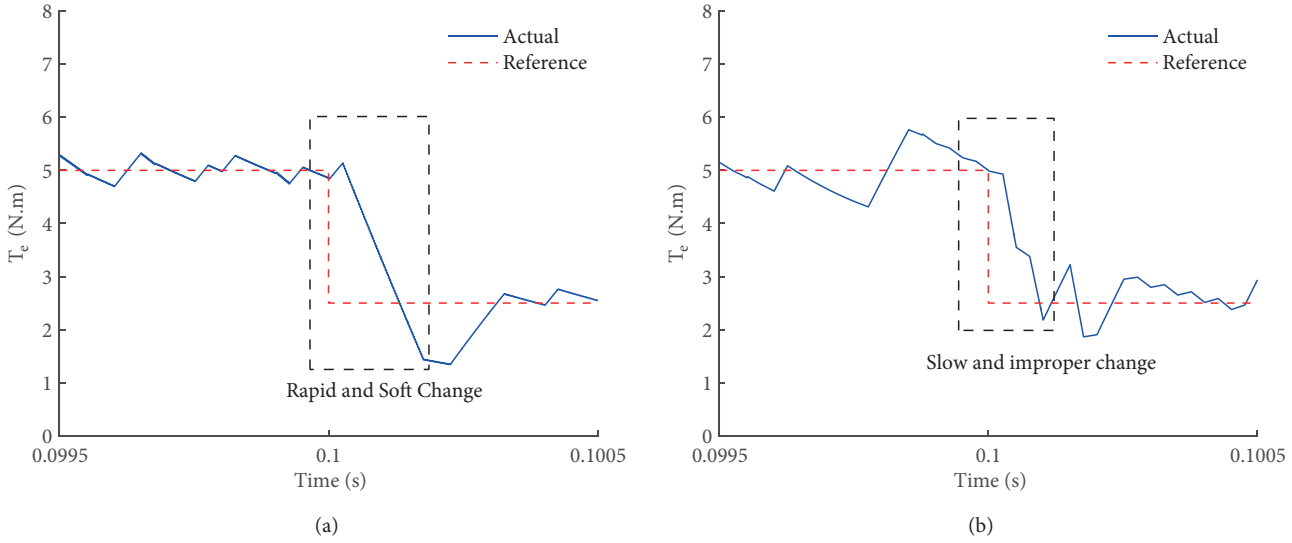

Figure 8. The electromagnetic torque waveform with the constant speed of 250 rpm with zoom: (a) the proposed method, (b) conventional.

resistance is the coefficient of T_s in predictive equations. Thus, it cannot affect the results with small values. Higher values increases the torque ripple because future estimations give wrong results. The speed is estimated by using Hall sensors. Thus, it is expected that the speed error increases when the future estimations have significant wrong values, as shown in Figure 12a. Stator winding inductance has a significant effect on torque ripple. However, the speed is estimated by using Hall sensors, and it is independent of torque variation, except its higher errors, as illustrated in Figure 12b. As can be inferred, the predictive controller tolerates 15% variation in stator winding resistance and stator winding inductance.

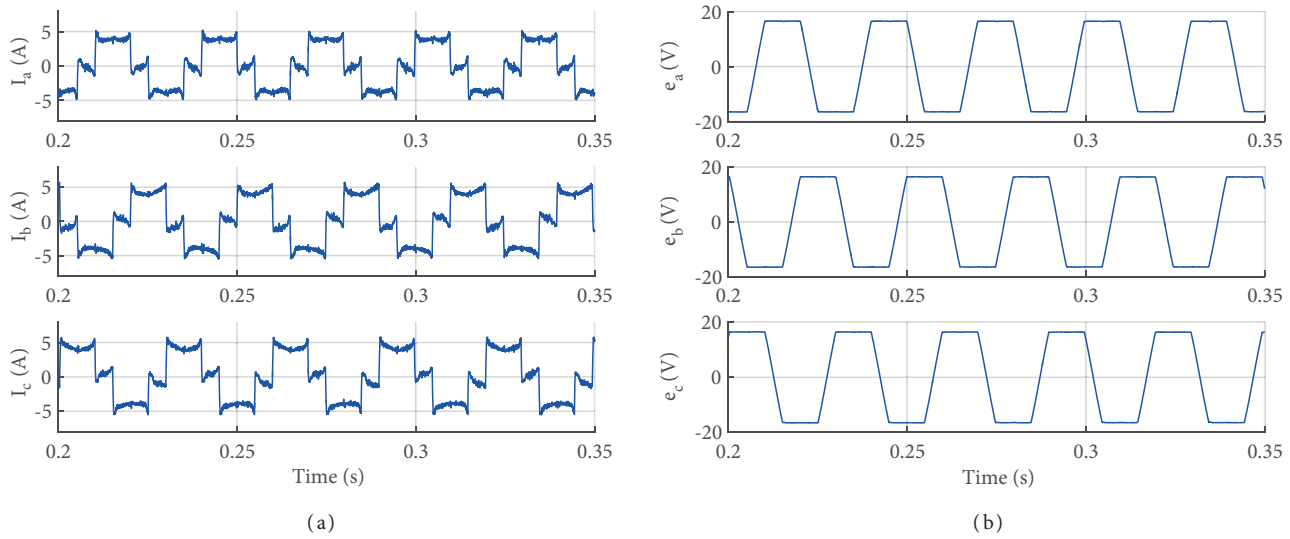

Figure 9. (a) The phase current waveforms with constant speed and torque of 250 rpm and 5 N.m, respectively, (b) the waveforms of back-emf with the constant speed and torque of 250 rpm and 5 N.m, respectively.

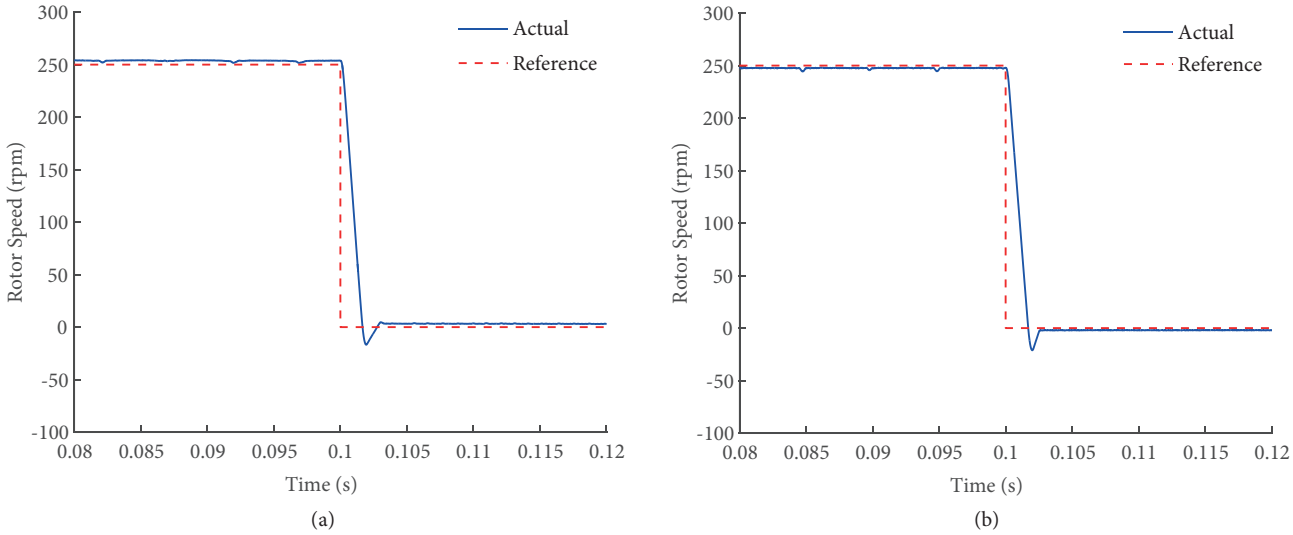

Figure 10. Brake mode at the constant torque of 5 N.m: (a) proposed controller, (b) conventional controller.

4. Conclusion

This paper proposes a new model predictive controller for BLDCM drives. It estimates the behavior of the controlled parameters, and after a simple process it generates a proper command for the six-switch inverter. Compared with the conventional current controller, this strategy shows better performance at the medium switching frequencies due to its predictive quality. It reduces the electromagnetic torque ripple up to 50%, which is suitable for smooth operation. This strategy increases the torque response rate up to 10% compared to the traditional controller. Furthermore, the proposed predictive current controller cancels the error between the actual speed and the rotor speed reference. Unlike the traditional current controller, this strategy decreases the impact of commutation time on the phase currents. The system efficiency is improved due to the ability to work with lower switching frequencies compared to the conventional method. The simplicity of the theory makes its implementation easy using digital signal processors or simple microcontrollers. As a result, the simulations

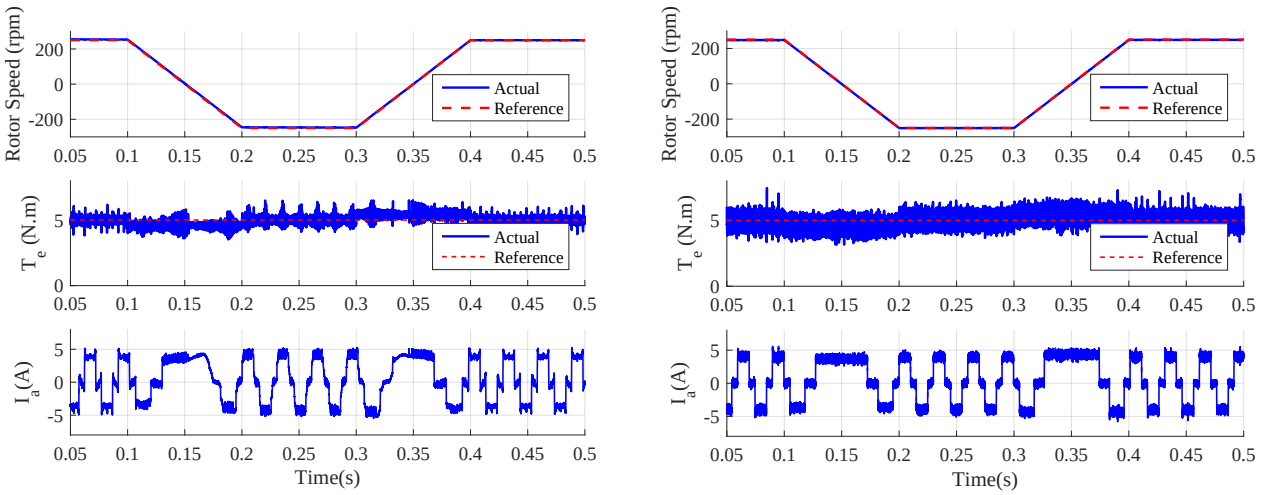

Figure 11. The effect of the rotor direction change: (a) predictive current controller, (b) conventional current controller.

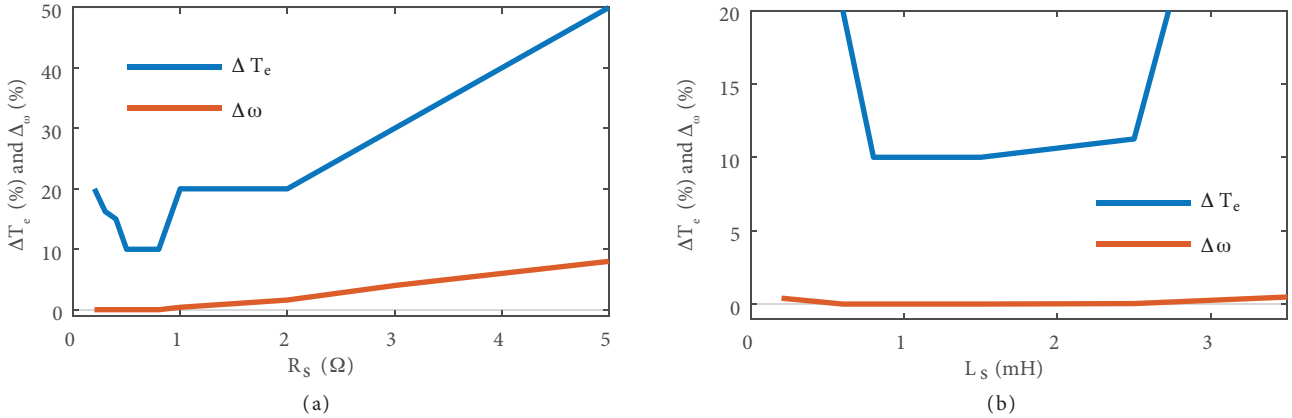

Figure 12. Stability analysis: (a) the effect of stator winding resistance, (b) the effect of stator winding inductance.

indicate that the proposed model predictive current controller performs better than the traditional current controller, and it is possible to test the performance and quality of this strategy in practical applications.

References

[1] Chau KT. Electric Vehicle Machines and Drives. 1st ed. Singapore: John Wiley & Sons, 2015.

[2] Chuang N, Gale TJ, Langman RA. Developing measuring inductance strategies on a direct current machine using a DC source with magnetic saturation. International Journal of Circuit Theory and Applications 2016; 44 (5): 1094-1111. doi: 10.1002/cta.2127

[3] Hosseinzadeh Soreshjani M, Abjadi N, Arab Markadeh G. A new arrangement of Z-source AC–AC converter and its closed-loop control system. International Journal of Circuit Theory and Applications 2015; 43 (10): 1491-1507. doi: 10.1002/cta.2023

[4] Liu S, Ge B, You X, Jiang X, Abu-Rub H et al. A novel quasi-Z-source indirect matrix converter. International Journal of Circuit Theory and Applications 2015; 43 (4): 438-454. doi: 10.1002/cta.1952

[5] Halvaei Niasar A, Moazzemi M. Design and implementation of direct power control system for brushless DC generator in standalone DC applications. Electric Power Components and Systems 2017; 45 (7): 752-762. doi: 10.1080/15325008.2017.1309722

[6] Yoon Y, Kim J. Precision control of a sensorless PM BLDC motor using PLL control algorithm. Electrical Engineering 2018; 100: 1097-1111. doi: 10.1007/s00202-017-0571-x

[7] Yilmaz M, Tuncay RN, Ustun O, Krein TP. Sensorless control of brushless DC motor based on Wavelet theory. Electric Power Components and Systems 2009; 37 (10): 1063-1080.

[8] Kim KH, Youn MJ. DSP-based high-speed sensorless control for a brushless DC motor using a DC link voltage control. Electric Power Components and Systems 2002; 30 (9): 889-906.

[9] Oksuztepe E, Omac Z, Kurum H. Sensorless vector control of PMSM with non-sinusoidal flux using observer based on FEM. Electrical Engineering 2014; 96 (3): 227-238.

[10] Paul AR, George M. Brushless DC motor control using digital PWM techniques. In: International Conference on Signal Processing, Communication, Computing and Networking Technologies; Thuckafay, India; 2011. pp. 733-738.

[11] Lee BK, Ehsani M, Advanced Simulation Model for Brushless DC Motor Drives. Electric Power Components and Systems 2003; 31 (9): 841-868.

[12] Xia C, Wu D, Shi T, Chen W. A current control scheme of brushless DC motors driven by four-switch three-phase inverters. IEEE Journal of Emerging and Selected Topics in Power Electronics 2017; 5 (1): 547-558.

[13] Hajiaghasi S, Salemnia A, Motabarian F. Four switches direct power control of BLDC motor with trapezoidal back-EMF. In: 8th Power Electronics, Drive Systems & Technologies Conference (PEDSTC); Mashhad, Iran; 2017. pp. 513-518.

[14] Shi T, Cao Y, Jiang G, Li X, Xia C. A torque control strategy for torque ripple reduction of brushless DC motor with nonideal back electromotive force. IEEE Transactions on Industrial Electronics 2017; 64 (6): 4423-4433. doi: 10.1109/TIE.2017.2674587

[15] Seguritan A, Rotunno M. Torque pulsation compensation for a DC motor using an extended Kalman filter approach. In: Proceedings of the 41st IEEE Conference on Decision and Control; Las Vegas, NV, USA; 2002. pp. 486-491.

[16] Kommula BN, Kota VR, A novel scheme for torque ripple minimization of BLDC motor used in solar air conditioner. Electrical Engineering 2018; 100: 2473-2483. doi:10.1007/s00202-018-0721-9

[17] Salah WA, Ishak D, Zneid BA, Abu Al Aish A, Jadin MS et al. Implementation of PWM control strategy for torque ripples reduction in brushless DC motors. Electrical Engineering 2015; 97 (3): 239-250.

[18] Liu Y, Zhu ZQ, Howe D. Commutation-torque-ripple minimization in direct-torque-controlled PM brushless DC drives. IEEE Transactions on Industrial Applications 2007; 43 (4): 1012-1021.

[19] Tarusan SAA, Jidin A, Huzainirah I, Rahim MK, Karim KA. DTC brushless DC motor by using constant switching frequency. In: IEEE International Conference on Power and Energy (PECon); Melaka, Malaysia; 2016. pp. 205-209.

[20] Nair DS, Jagadanand G, George S. Analysis of direct torque controlled BLDC motor with reduced torque ripple. In: IEEE International Conference on Signal Processing, Informatics, Communication and Energy Systems (SPICES); Kozhikode, India; 2015. pp. 1-5.

[21] Nguyen DD, Ta MC. New Direct Torque Control Scheme for BLDC Motor Drives Suitable for EV Applications. In: IEEE Vehicle Power and Propulsion Conference (VPPC); Coimbra, Portugal; 2014. pp. 1-5. doi: 10.1109/VPPC.2014.7007109

[22] Muthu R, Kumaran MR, Rajaraman LAA, Ganesh P, Reddy PGP. Direct Torque Control of matrix converter fed BLDC motor. In: IEEE 6th India International Conference on Power Electronics (IICPE); Kurukshetra, India; 2014. pp. 1-6.

[23] Noroozi MA, Moghani JS, Monfared JM, Givi H. An improved direct torque control of brushless DC motors using twelve voltage space vectors. In: 3rd Power Electronics and Drive Systems Technology (PEDSTC); Tehran, Iran; 2012. pp. 133-138.

[24] Ozturk SB, Alexander WC, Toliyat HA. Direct torque control of four-switch brushless DC motor with non-sinusoidal back EMF. IEEE Transactions on Power Electronics 2010; 25 (2): 263-271.

[25] Ozturk SB, Toliyat HA. Direct Torque Control of Brushless DC Motor with Non-sinusoidal Back-EMF. In: IEEE International Electric Machines & Drives Conference; Antalya, Turkey; 2007. pp. 165-171.

[26] Yong L, Zhu ZQ, Howe D. Direct torque control of brushless DC drives with reduced torque ripple. IEEE Transactions on Industry Applications 2005; 41 (2): 599-608. doi: 10.1109/TIA.2005.844853

[27] Siami M, Khaburi DA, Rodriguez J. Simplified finite control set-model predictive control for matrix converter-fed PMSM drives. IEEE Transactions on Power Electronics 2018; 33 (3): 2438-2446.

[28] Wang F, Mei X, Tao P, Kennel R, Rodriguez J. Predictive field-oriented control for electric drives. Chinese Journal of Electrical Engineering 2017; 3 (1): 73-78. doi: 10.23919/CJEE.2017.7961324

[29] Wang F, Mei X, Rodriguez J, Kennel R. Model predictive control for electrical drive systems-an overview. CES Transactions on Electrical Machines and Systems 2017; 1 (3): 219-230.

[30] Vazquez S, Rodriguez J, Rivera M, Franquelo LG, Norambuena M. Model predictive control for power converters and drives: advances and trends. IEEE Transactions on Industrial Electronics 2017; 64 (2): 935-947.

[31] Valle RL, Almeida PMD, Ferreira AA, Barbosa PG. Unipolar PWM predictive current-mode control of a variable-speed low inductance BLDC motor drive. IET Electric Power Applications 2017; 11 (5): 688-696.

[32] Siami M, Khaburi DA, Rivera M, Rodriguez J. A computationally efficient lookup table based FCS-MPC for PMSM drives fed by matrix converters. IEEE Transactions on Industrial Electronics 2017; 64 (10): 7645-7654.

[33] Siami M, Khaburi DA, Rivera M, Rodriguez J. An experimental evaluation of predictive current control and predictive torque control for a PMSM fed by a matrix converter. IEEE Transactions on Industrial Electronics 2017; 64 (11): 8459-8471.

[34] Zhang Y, Xia B, Yang H, Rodriguez J. Overview of model predictive control for induction motor drives. Chinese Journal of Electrical Engineering 2016; 2 (1): 62-76.

[35] Garcia C, Rodriguez J, Silva C, Rojas C, Zanchetta P et al. Full predictive cascaded speed and current control of an induction machine. IEEE Transactions on Energy Conversion 2016; 31 (3): 1059-1067. doi: 10.1109/TEC.2016.2559940

[36] Zhou D, Zhao J, Liu Y. Predictive torque control scheme for three-phase four-switch inverter-fed induction motor drives with DC-link voltages offset suppression. IEEE Transactions on Power Electronics 2015; 30 (6): 3309-3318.

[37] Rojas CA, Rodriguez J, Villarroel F, Espinoza JR, Silva CA et al. Predictive torque and flux control without weighting factors. IEEE Transactions on Industrial Electronics 2013; 60 (2): 681-690. doi: 10.1109/TIE.2012.2206344

[38] Lahooti Eshkevari A, Mosallanejad A, Sepasian MS. Design and analysis of a simple predictive power controller for a 1.0-kV single-phase NPC PWM rectifier. International Journal of Circuit Theory and Applications 2018; 46 (12): 2495-2511.